The Annals of Applied Statistics
2023, Vol. 17, No. 3, 2305–2325
https://doi.org/10.1214/22-AOAS1719

SPATIAL QUANTILE AUTOREGRESSION FOR SEASON WITHIN YEAR DAILY MAXIMUM TEMPERATURE DATA

BY JORGE CASTILLO-MATEO[1,a], JESÚS ASÍN[1,b], ANA C. CEBRIÁN[1,c], ALAN E. GELFAND[2,e] AND JESÚS ABAURREA[1,d]

[1]*Department of Statistical Methods, University of Zaragoza,* [a]*jorgecm@unizar.es,* [b]*jasin@unizar.es,* [c]*acebrian@unizar.es,* [d]*abaurrea@unizar.es*

[2]*Department of Statistical Science, Duke University,* [e]*alan@stat.duke.edu*

Regression is the most widely used modeling tool in statistics. Quantile regression offers a strategy for enhancing the regression picture beyond customary mean regression. With time-series data, we move to quantile autoregression and, finally, with spatially referenced time series, we move to space-time quantile regression. Here, we are concerned with the spatiotemporal evolution of daily maximum temperature, particularly with regard to extreme heat. Our motivating data set is 60 years of daily summer maximum temperature data over Aragón in Spain. Hence, we work with time on two scales—days within summer season across years—collected at geocoded station locations. For a specified quantile, we fit a very flexible, mixed-effects autoregressive model, introducing four spatial processes. We work with asymmetric Laplace errors to take advantage of the available conditional Gaussian representation for these distributions. Further, while the autoregressive model yields conditional quantiles, we demonstrate how to extract marginal quantiles with the asymmetric Laplace specification. Thus, we are able to interpolate quantiles for any days within years across our study region.

1. Introduction. Quantile regression (QR) has a rich history by now, dating to Koenker and Bassett (1978), with much seminal work by Koenker and colleagues (see, e.g., Koenker and Machado (1999), Koenker (2005), Koenker and Xiao (2006)). Many facets are considered in the literature including choice of optimization function (equivalently error distribution), dependence through autoregression, and quantile crossing. We review this literature briefly below. Here, our contribution is to consider QR in the context of a complex spatiotemporal model. This model specifies temporal dependence through autoregression, adopting two time scales, and introduces needed spatial dependence through four Gaussian processes (GPs). We are motivated by mean modeling work developed in Castillo-Mateo et al. (2022) but now seeking quantiles associated with time series of daily *maximum* temperature during the summer season over a period of 60 years. We use data obtained from monitoring stations in the Comunidad Autónoma de Aragón, Spain. Our interest is in extreme heat; specifically, we work with daily maximum temperatures and primarily inferential focus on the $\tau = 0.95$ quantile. Throughout the paper, when we refer to temperature it is a daily maximum temperature. However, our model could be applied to arbitrary quantiles of, for example, daily average temperature or daily minimum temperature.

More precisely, we specify a spatial conditional autoregression model on a daily scale using the asymmetric Laplace (AL) distribution. Our quantile autoregression is an AR(1) form, producing conditional temperature quantiles given the previous day's temperature. The specification enables spatial autoregression at daily and annual scale. We first present the

Received January 2022; revised November 2022.
Key words and phrases. Asymmetric Laplace distribution, Gaussian process, hierarchical model, marginal quantile, Markov chain Monte Carlo, seasonal time series.

inference associated with the conditional model, discussing the resulting conditional quantiles and employing model performance assessment by location. The conditional quantiles facilitate assessment of persistence, for example, according to yesterday's temperature, what are today's temperature quantiles? Next, we offer an attractive approach to obtain marginal quantiles at daily scale. The marginal quantiles enable interpolation. We can show the spatial surface for a given marginal quantile. We can also consider averaging to provide marginal quantiles associated with say, 7-day average temperatures. We consider these both spatially and also dynamically. In fact, we show how to provide marginal quantiles associated with 7-day averages over a specified region. We work in a hierarchical Bayesian framework, enabling full posterior inference for all of the quantiles we develop.

There are two modeling approaches for QR in the literature. The first follows the original ideas by Koenker and Bassett (1978) and offers a separate regression model for each of the quantiles of interest. This approach is usually called *multiple* QR, and inference typically proceeds by minimizing a check loss function or assuming an AL error term. Examples of multiple QR with AL errors appear in Yu and Moyeed (2001) while Kozumi and Kobayashi (2011) present a Gibbs sampler for a Bayesian QR model. The second approach, which is usually called *joint* QR, specifies an appropriate joint model for all quantiles (see, e.g., Tokdar and Kadane (2012), Yang and Tokdar (2017), Das and Ghosal (2017a)). Broad implementation for joint QR has proven challenging.

We can also classify the models in terms of whether they incorporate temporal, spatial, or spatiotemporal dependence. Koenker and Xiao (2006) established the basis for joint quantile autoregression (QAR) models in time series. A detailed overview of the different strands of time-series QR modeling can be found in Peters (2018). Recently, spatial quantiles have been an active area of research. Hallin, Lu and Yu (2009) introduce spatial multiple QR that is nonparametric, focusing on asymptotic behavior using assumptions associated with time-series asymptotics. Reich, Fuentes and Dunson (2011) develop a spatial joint QR model that incorporates spatial dependence through spatially varying regression coefficients, which are expressed as a weighted sum of Bernstein basis polynomials where the weights are constrained spatial GPs. Lum and Gelfand (2012) consider spatial multiple QR with AL errors and then extend it to capture spatial dependence by introducing the AL process. Yang and He (2015) consider a nonparametric approach based on Bayesian spatial QR using empirical likelihood as a working likelihood and spatial priors. Chen and Tokdar (2021) specify a spatial joint QR based on the so-called constraint-free reparametrization by generalizing the model of Yang and Tokdar (2017) and characterizing spatial dependence via a Gaussian or t-copula process on the underlying quantile levels of the observation units. Spatiotemporal quantile models are the most challenging and little work has been done in that regard. For example, Reich (2012) follows Reich, Fuentes and Dunson (2011), but allows for residual correlation via a spatiotemporal copula model. Neelon et al. (2015) propose a multiple QR model for areal data. They model the random effects via intrinsic conditionally autoregressive priors, and they adopt the Bayesian approach based on the AL errors. Das and Ghosal (2017b) develop a joint QR model with a single explanatory variable following the representation of quantile functions given by Tokdar and Kadane (2012) and Das and Ghosal (2017a). The explanatory variable is a linear trend over time and spatial dependence is captured by a B-spline basis expansion prior.

The primary advantage of joint QR models is that they avoid the possibility of quantile crossing. This can occur in methods that estimate and infer about quantiles separately. However, joint methods have the disadvantage of restrictive assumptions on covariates and very demanding computation. Further, suppose we work with quantiles of an error distribution such as the AL, that is, we model $Y = \mu_\tau + \epsilon_\tau$ where the distribution for ϵ_τ has zero as the τ quantile. Therefore, $P(\epsilon_\tau \leq 0) = \tau$ so μ_τ provides a τ-QR for Y. If we model in this

way, we impose a *soft* (stochastic) order on the quantiles. More precisely, if we also write $Y = \mu_{\tau^*} + \epsilon_{\tau^*}$ with $\tau < \tau^*$, then ϵ_{τ^*} will be stochastically smaller than ϵ_τ, equivalently μ_{τ^*} will be stochastically larger than μ_τ, yielding the stochastic order.

Recently, QR models have become widely used in climate studies (see, e.g., Haugen et al. (2018), McKinnon and Poppick (2020)). Gao and Franzke (2017) fit a local joint QR to analyze the spatial and temporal pattern of extreme daily temperature. The Bayesian spatiotemporal quantile model in Reich (2012) is used by Tan, Gan and Chen Shu Liu (2019) to identify climate changes in accumulated precipitation in Canada. None of those models include serial dependence in daily variables, but Yang, Li and Xu (2018) propose a semiparametric autoregressive QR model including lagged data to estimate the thresholds to define quantile-based temperature extreme indices.

Our interest focuses on the analysis of the temporal evolution of the distributional changes in the daily maximum temperatures during the summer periods from 1956 to 2015 around the Comunidad Autónoma de Aragón, in the northeast of Spain. The region includes part of the Ebro Valley in the center, with mountainous areas in the south (Iberian System) and the north (Pyrenees). Despite its relatively small size, the region shows a diverse orography, with a warm homogeneous climate in the center and greater climatic variability in the mountainous areas.

Lastly, in this article we discuss many different quantiles—empirical and modeled, marginal and conditional (perhaps conditioned on a marginal quantile). So, we offer some notation to hopefully help in what follows. Our primary model is for a spatial QAR in the form of conditional quantiles. So, we define $Q_V(\tau \mid y)$ as the τ quantile for variable V given y. Hence, for example, $Q_{Y_{t\ell}(\mathbf{s})}(\tau \mid Y_{t,\ell-1}(\mathbf{s}))$ is the τ conditional quantile for the daily temperature variable for day ℓ in year t at location $\mathbf{s}$ given the previous day's temperature at that site. Also, y might be an empirical quantile as we clarify below. Marginal quantiles, extracted from our spatial QAR (employing adjustment), are denoted by $\tilde{q}_V(\tau)$. So, $\tilde{q}_{Y_{t\ell}(\mathbf{s})}(\tau)$ is the τ marginal quantile for the daily temperature variable for day ℓ in year t at location $\mathbf{s}$. Empirical quantiles are denoted by $q_V^{\text{emp}}(\tau^*)$. They may be indexed by site, averaged over days within a year, years for a given day, or both. When they appear, an explicit definition is clarified in the associated text. They may be used in specifying a conditional quantile and, in this case, τ^* need not equal τ.

The format of the paper is as follows. Section 2 describes the data set with some descriptive work. Section 3 presents our spatial QAR model with the results of the model fitting and some model adequacy assessment. Section 4 develops a strategy for extracting marginal quantiles from our QAR model and then develops interpolation and averaging over time and space for them. Section 5 concludes with a summary and future work.

2. The data. The analyses presented here consider daily maximum temperature (°C) data at $n = 18$ sites around the Comunidad Autónoma de Aragón (see Figure 1) provided by the Agencia Estatal de Meteorología (AEMET) in Spain. The data are available at a daily scale from 1956 to 2015, but the focus of the analyses is in the warm months of June, July, and August (denoted as JJA); in this regard, we fit the models with data in an extended period from May 1 to September 30 to avoid boundary issues.

The region of interest, $\mathcal{D}$, is around Aragón, located in the Ebro Basin in northeastern Spain, with a spatial extent of roughly 53,000 km^2. In particular, $\mathcal{D}$ has corners at approximately (40.5°N, 1.7°W), (42.9°N, 1.7°W), (42.9°N, 0.0°E), and (40.5°N, 0.0°E). Figure 1 shows the name, location, and elevation of the 18 sites. The Ebro River flows from the northwest to the southeast through a valley bordered by the Pyrenees and the Cantabrian Range in the north and the Iberian System in the southwest. The maximum elevation is around 3000 m in the Pyrenees, 2000 m in the Cantabrian Range and the Iberian System, while the elevation

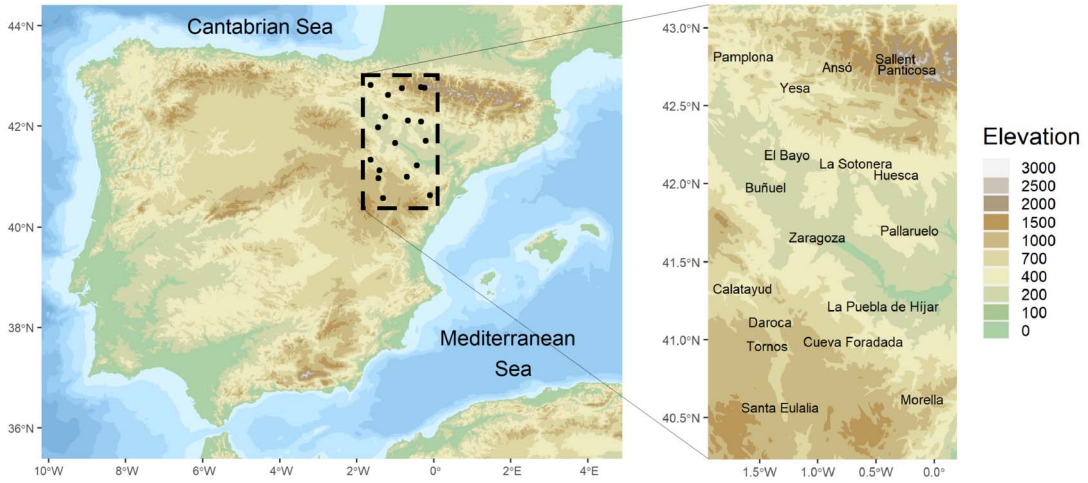

FIG. 1. *Location of the* 18 *sites around the Comunidad Autónoma de Aragón in northeastern Spain.*

in the Central Valley varies between 200–400 m. In summary, roughly 62% of the area is above 500 m and 28% above 1000 m.

According to AEMET (2011), the central part of the Valley is characterized by a Mediterranean-continental dry climate with irregular rainfall and a large temperature range. However, several climate subareas can be distinguished due to the heterogeneous orography and other influences. Consequently, the region presents a wide variety of climate conditions in a relatively small area, bringing interest in studying it and challenge in modeling it.

With regard to showing maps over this region, $\mathcal{D}$ was partitioned with a resolution of 4 km $\times$ 4 km grid cells yielding $K = 2342$ cells.

2.1. *Descriptive analysis.* Figure 2 describes the distribution across sites of three features related to the empirical quantiles of daily temperatures in JJA months for a grid of quantiles. Each boxplot corresponds to a quantile and is based on 18 points, one point for each observed site. The first plot shows the empirical quantiles calculated with 60 (years) $\times$ 92 (days) observations, that is, each one of the 18 points corresponds to the empirical quantile across 60×92 observations, and each boxplot is across 18 empirical quantiles from the 18 sites. The range of each boxplot varies around 10°C to 15°C, and the difference between the median of the 0.95 and 0.05 quantiles is around 15°C, indicating a similar variability across sites and across quantiles. The second plot shows the difference between the empirical quantiles of the 30-year periods 1986–2015 and 1956–1985 so that each quantile is now calculated with 30×92

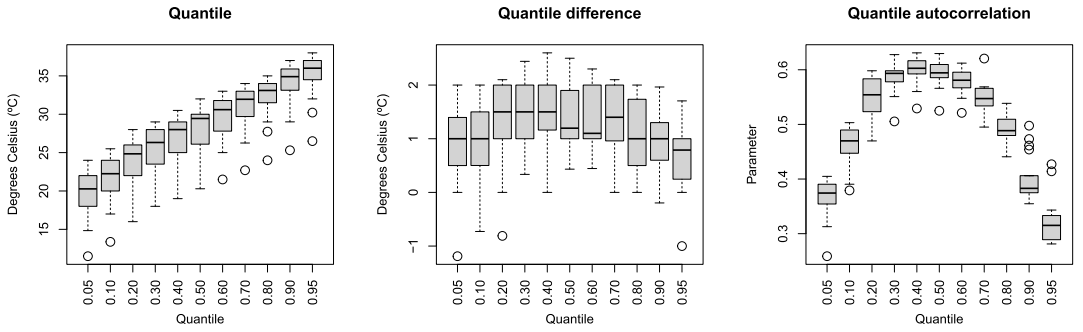

FIG. 2. *Boxplots of the* 18 *sites across quantiles to describe empirical quantile features.*

observations. Most of the observed increases vary from around -0.5°C to 2.5°C, but the observed warming is higher in central quantiles. The variability of this increase across quantiles is lower than across sites. The third plot shows the quantile autocorrelation, a measure of quantile dependence based on the correlation between a binary variable indicating whether the temperature in a day is higher than its empirical quantile and the previous day's temperature; see Li, Li and Tsai (2015) and Section S1.1 in the Supplementary Material (Castillo-Mateo et al. (2023)) for the details. This autocorrelation is strong in all sites and quantiles, but it clearly decreases in both tails. The variability across quantiles is larger than across sites. Section S1.1 also includes a descriptive analysis of a second-order quantile autocorrelation, with little or no evidence in favor of including it in the model.

A thorough analysis of the temporal pattern and the effect of elevation and latitude in the quantiles of temperatures is offered in Section S1.2 of the Supplementary Material. This analysis shows that elevation of the site has a roughly negative linear relationship in the empirical quantiles and that this effect is slightly higher in the left tail. As expected, given the size of the region, no latitudinal gradient is observed. Lastly, the data show a strong seasonal component, with no evidence of changes across quantiles and across time. The increase observed between both 30-year periods is homogeneous during the summer, although relevant differences are observed across sites and quantiles.

3. The spatial quantile autoregression model.

3.1. *Review of the asymmetric Laplace distribution.* We introduce the AL distribution as an error distribution for multiple QR models using the following parametrization. We denote by $\epsilon \sim \mathrm{AL}(\mu, \sigma, \tau)$ a random variable with probability density function (pdf),

$$f(\epsilon \mid \mu, \sigma, \tau) = \sigma\tau(1-\tau)\begin{cases}\exp\{-(1-\tau)\sigma|\epsilon-\mu|\} & \text{if } \epsilon < \mu,\\ \exp\{-\tau\sigma|\epsilon-\mu|\} & \text{if } \epsilon \geq \mu.\end{cases}$$

The cumulative distribution function is

$$F(\epsilon \mid \mu, \sigma, \tau) = \begin{cases}\tau\exp\{-(1-\tau)\sigma|\epsilon-\mu|\} & \text{if } \epsilon < \mu,\\ 1-(1-\tau)\exp\{-\tau\sigma|\epsilon-\mu|\} & \text{if } \epsilon \geq \mu.\end{cases}$$

Here, μ is a location parameter, $\sigma > 0$ is a scale parameter, and $\tau \in (0, 1)$ is an asymmetry parameter. In particular, it is easily checked that μ is the τ quantile of the distribution and we will typically set $\mu = 0$ so that $P(\epsilon \leq 0) = \tau$.

The pdf above can be rewritten as $f(\epsilon \mid \mu, \sigma, \tau) = \sigma\tau(1-\tau)\exp\{-\sigma\delta_\tau(\epsilon-\mu)\}$ where $\delta_\tau(u) = u(\tau - \mathbf{1}(u < 0))$ is the *check loss* function (Koenker and Bassett (1978)). For a sample $\{x_i : i = 1, \ldots, n\}$, finding $\arg\min_\mu \sum \delta_\tau(x_i - \mu)$ returns the τ empirical quantile. Just as minimizing the sum of squares loss is associated with normal errors, minimizing check loss is associated with AL errors.

A convenient strategy for generating $\epsilon \sim \mathrm{AL}(0, \sigma, \tau)$ variables is to use the following representation proven by comparing moment generating functions (see, e.g., Kotz, Kozubowski and Podgórski (2001)). We can express ϵ in terms of

$$\epsilon = \sqrt{\frac{2U}{\sigma^2\tau(1-\tau)}}Z + \frac{1-2\tau}{\sigma\tau(1-\tau)}U,$$

where $Z \sim N(0, 1)$ and $U \sim \mathrm{Exp}(1)$. So,

$$\epsilon \mid \sigma, U \sim N\left(\frac{1-2\tau}{\sigma\tau(1-\tau)}U, \frac{2U}{\sigma^2\tau(1-\tau)}\right) \tag{1}$$

is normally distributed enabling us to use all of the familiar Gaussian theory.

3.2. *The space-time model.* Let $\tau \in (0,1)$ denote a quantile order, where each quantile is modeled separately. Our general form for a spatiotemporal τ-QAR with two time scales is given by

$$
\begin{aligned}
Y_{t\ell}(\mathbf{s}) &= Q_{Y_{t\ell}(\mathbf{s})}\big(\tau \mid Y_{t,\ell-1}(\mathbf{s})\big) + \epsilon^{\tau}_{t\ell}(\mathbf{s}) \\
&= q^{\tau}_{t\ell}(\mathbf{s}) + \rho^{\tau}(\mathbf{s})\big(Y_{t,\ell-1}(\mathbf{s}) - q^{\tau}_{t,\ell-1}(\mathbf{s})\big) + \epsilon^{\tau}_{t\ell}(\mathbf{s}),
\end{aligned} \tag{2}
$$

where $Q_{Y_{t\ell}(\mathbf{s})}(\tau \mid Y_{t,\ell-1}(\mathbf{s}))$ is the τ conditional quantile of $Y_{t\ell}(\mathbf{s})$ given $Y_{t,\ell-1}(\mathbf{s})$ and the error term is $\epsilon^{\tau}_{t\ell}(\mathbf{s}) \sim$ ind. AL$(0, \sigma^{\tau}(\mathbf{s}), \tau)$. Here, $q^{\tau}_{t\ell}(\mathbf{s})$ contains fixed and random effects as below. In addition, $\rho^{\tau}(\mathbf{s})$ is a spatially varying autoregression coefficient and $\sigma^{\tau}(\mathbf{s})$ is a spatially varying pure error scale parameter at location $\mathbf{s}$.

Based upon the foregoing exploratory analysis along with that developed in Castillo-Mateo et al. (2022), we adopt an analogue of their spatiotemporal mean autoregression model. Here, $Y_{t\ell}(\mathbf{s})$ denotes the daily maximum temperature for day ℓ, $\ell = 2, \ldots, L$ of year t, $t = 1, \ldots, T$ at location $\mathbf{s}$, $\mathbf{s} \in \mathcal{D}$, the study region. We specify $\rho^{\tau}(\mathbf{s})$ to capture spatial autoregession dependence through the GP $Z^{\tau}_{\rho}(\mathbf{s}) = \log\{(1+\rho^{\tau}(\mathbf{s}))/(1-\rho^{\tau}(\mathbf{s}))\}$ with mean Z^{τ}_{ρ} and exponential covariance function having variance parameter $\sigma^{2,\tau}_{\rho}$ and decay parameter ϕ^{τ}_{ρ}. In the same manner, we specify $\sigma^{\tau}(\mathbf{s})$ to capture spatial scale dependence through the GP $Z^{\tau}_{\sigma}(\mathbf{s}) = \log\{\sigma^{\tau}(\mathbf{s})\}$ with mean Z^{τ}_{σ} and exponential covariance function having variance parameter $\sigma^{2,\tau}_{\sigma}$ and decay parameter ϕ^{τ}_{σ}.

As for $q^{\tau}_{t\ell}(\mathbf{s})$, we adopt

$$
q^{\tau}_{t\ell}(\mathbf{s}) = \beta^{\tau}_0 + \alpha^{\tau} t + \beta^{\tau}_1 \sin(2\pi\ell/365) + \beta^{\tau}_2 \cos(2\pi\ell/365) + \beta^{\tau}_3 \,\mathrm{elev}(\mathbf{s}) + \gamma^{\tau}_t(\mathbf{s}),
$$

where $\gamma^{\tau}_t(\mathbf{s}) = \beta^{\tau}_0(\mathbf{s}) + \alpha^{\tau}(\mathbf{s})t + \psi^{\tau}_t + \eta^{\tau}_t(\mathbf{s})$. The *fixed effects* are given by β^{τ}_0, a global intercept, $\alpha^{\tau} t$, a global long-term linear trend, sin and cos terms that provide the annual seasonal component, and elev$(\mathbf{s})$, the elevation at $\mathbf{s}$. The *random effects* given by $\gamma^{\tau}_t(\mathbf{s})$ capture space-time dependence through GPs. In particular, $\beta^{\tau}_0(\mathbf{s})$ is a GP with zero mean and exponential covariance function having variance parameter $\sigma^{2,\tau}_{\beta_0}$ and decay parameter $\phi^{\tau}_{\beta_0}$, and it provides a local spatial adjustment to the intercept. The $\alpha^{\tau}(\mathbf{s})$ are a GP, with zero mean and exponential covariance function having variance parameter $\sigma^{2,\tau}_{\alpha}$ and decay parameter ϕ^{τ}_{α}, to provide a local slope adjustment to the linear trend. Together, $\gamma_t(\mathbf{s})$ supplies a *locally linear* trend, an exceptionally rich spatial specification. With the inclusion of seasonality, it is difficult to imagine that the data could inform about a higher-order local choice. Continuing, $\psi^{\tau}_t \sim$ i.i.d. $N(0, \sigma^{2,\tau}_{\psi})$ provides annual intercepts to allow for yearly shifts (i.e., for hotter or colder years),[1] and $\eta^{\tau}_t(\mathbf{s}) \sim$ i.i.d. $N(0, \sigma^{2,\tau}_{\eta})$ provides local annual intercepts to allow for local yearly shifts.

We make two further points here. Focusing on performance of conditional quantiles, we have investigated departures from our first-order regression but have found no reason to adopt a more elaborate ARMA specification. In the exploratory and residual analysis, no evidence of second-order correlation has been found while dependence explained by MA terms becomes confusing with regard to our conditional objective. Second, we do not introduce spatial variability in the seasonality in our study. We are interested in the warmest time of the year, JJA. Our region is small enough to assume that the daily amplitude of solar incidence, that is, seasonality, during JJA is almost equivalent between the northernmost and southernmost sites. A brief residual analysis to validate the seasonal term used in the model is given in Section S2 of the Supplementary Material.

[1] An autoregression could be considered for ψ^{τ}_t. However, Castillo-Mateo et al. (2022) found no such autocorrelation in their means model.

We conclude with a technical remark regarding the validity of the Bayesian analysis for individual quantiles based on the working AL likelihood since this likelihood differs from that of the data generating process. Sriram, Ramamoorthi and Ghosh (2013) established sufficient conditions for the posterior consistency of model parameters under the AL working likelihood (at a single quantile level). The situation is more complicated when multiple quantile levels are considered, as this means different likelihoods will be utilized in each of the Bayesian analyses. When the AL likelihood differs from the data generating process, there is some literature providing posterior adjustments under the linear quantile regression model for independent data (see, e.g., Chernozhukov and Hong (2003), Yang, Wang and He (2016)). While it is useful to be aware of these issues, addressing them is beyond the scope of our complex spatiotemporal modeling employed here.

3.2.1. *Prior distributions and model fitting.* Model inference is implemented in a Bayesian framework. To complete the model, we specify prior distributions for all model parameters. In this setting, diffuse and, when available, conditionally conjugate prior distributions are chosen. Recall that the model adopts a conditional AL distribution for all $Y_{t\ell}(\mathbf{s})$, and that this distribution can be expressed as normal when it is conditioned on $U^{\tau}_{t\ell}(\mathbf{s}) \sim \text{Exp}(1)$. Therefore, the coefficient parameters β^{τ}_0, α^{τ}, β^{τ}_1, β^{τ}_2, and β^{τ}_3 are each assigned independent normal prior distributions with mean 0 and standard deviation 100. The variance parameters, $\sigma^{2,\tau}_{\psi}$ and $\sigma^{2,\tau}_{\eta}$, are assigned independent Inverse-Gamma$(0.1, 0.1)$ prior distribution.

The specification of the GPs is as follows. First, Z_{ρ} and Z_{σ} are each given a normal prior distribution with mean 0 and standard deviation 100. Second, the variance parameter for each of the four spatial covariances, $\sigma^{2,\tau}_{\beta_0}$, $\sigma^{2,\tau}_{\alpha}$, $\sigma^{2,\tau}_{\rho}$, and $\sigma^{2,\tau}_{\sigma}$, is assigned an independent Inverse-Gamma$(0.1, 0.1)$ prior distribution. With an exponential covariance function, the product of the variance and the decay parameter is identified but the individual parameters are not (Zhang (2004)). With stronger interest in the spatial variability, we adopt weak priors and let the data inform about the σ^2's. We are more precise with regard to the decay parameters. In fact, with information well informed by the spatial scale of our study region, we fix the decay parameters $\phi \equiv \phi^{\tau}_{\beta_0} = \phi^{\tau}_{\alpha} = \phi^{\tau}_{\rho} = \phi^{\tau}_{\sigma} = 3/d_{\max}$, where $d_{\max}$ is the maximum distance between any pair of spatial locations. That is, with an exponential covariance function, the decay parameter is 3/range, and it is set to the value associated with the largest spatial range for the observed data locations.

We develop a Metropolis-within-Gibbs algorithm to obtain Markov chain Monte Carlo (MCMC) samples from the joint posterior distribution. In particular, we derive full conditional distributions for each of the parameters, including the $n \times T \times (L-1)$ latent exponential variables $\xi^{\tau}_{t\ell}(\mathbf{s}) = U^{\tau}_{t\ell}(\mathbf{s})/\sigma^{\tau}(\mathbf{s})$. This parametrization is adopted to obtain a gamma full conditional distribution for the scale parameter in the AL (Kozumi and Kobayashi (2011)). However, in our case, with a GP prior for the log-scale parameter, the full conditional is still nonstandard so we do not benefit from this parametrization. For the fitting, we introduce $\tilde{\beta}^{\tau}_0(\mathbf{s}) = \beta^{\tau}_0 + \beta^{\tau}_0(\mathbf{s})$ and $\tilde{\alpha}^{\tau}(\mathbf{s}) = \alpha^{\tau} + \alpha^{\tau}(\mathbf{s})$ within $\gamma^{\tau}_t(\mathbf{s})$ to enable the benefits of hierarchical centering in the model fitting (Gelfand, Sahu and Carlin (1995)). Details of the Gibbs sampler used for the model fitting are provided in Section S3 of the Supplementary Material. All the covariates have been centered and scaled to have mean zero and standard deviation one to improve the mixing of the algorithm.

3.3. *Results of model fitting.* This section summarizes the results of the QAR models for $\tau \in \{0.05, 0.10, 0.20, \ldots, 0.80, 0.90, 0.95\}$ quantiles fitted to the temperature series described in Section 2. The parameters $\alpha^{\tau}, \beta^{\tau}_1, \beta^{\tau}_2, \beta^{\tau}_3, \alpha^{\tau}(\mathbf{s})$, and σ^{τ}_{α} have been rescaled to interpret them in terms of the original scales of the covariates. For each τ, using MCMC and the Gibbs sampling algorithm (see Section S3), we ran three chains, each with different initial

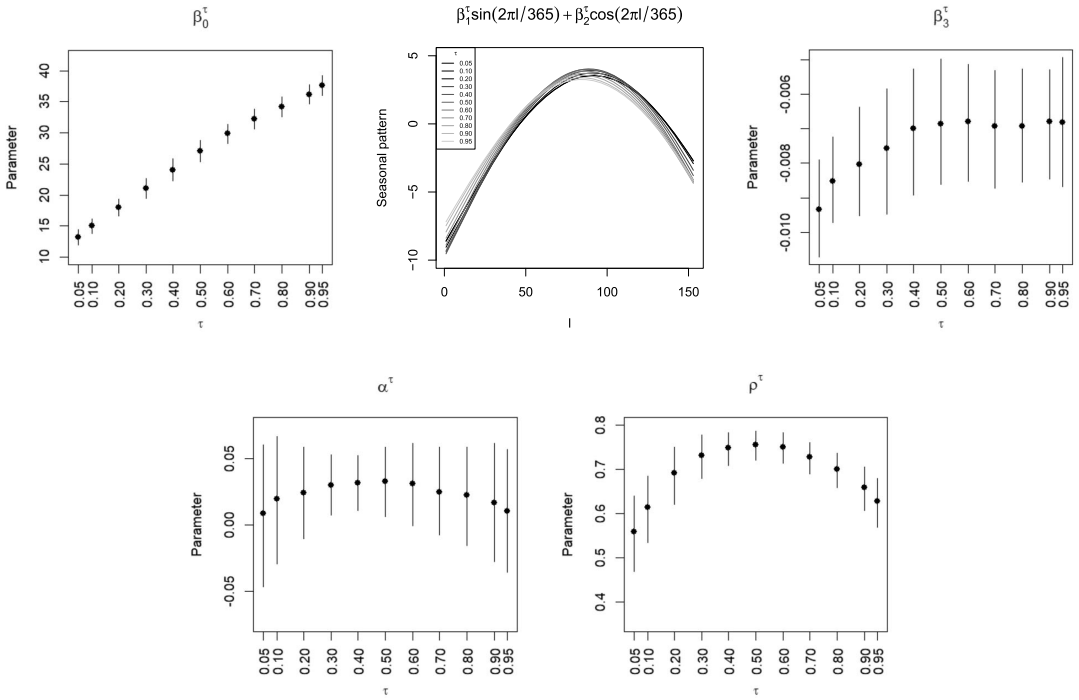

FIG. 3. *Posterior median and* 90% *credible interval of the main parameters and posterior mean of the centered seasonal pattern captured by the harmonic terms* (*first row central plot*) *across quantiles*.

values, out to 1,000,000 iterations for each chain, to obtain samples from the joint posterior distribution. The first 100,000 samples were discarded as burn-in and the remaining 900,000 samples were thinned to retain 1000 samples from each chain for posterior inference. Experiments were run on a computer with an Intel Core i9-10900K processor running at 3.70 GHz using 64 GB of RAM, running Windows 10 Pro version 21H2. Under this setup, fitting eleven models in parallel, we were able to fit the 3 (chains) $\times$ 11 (τ's) models in 3×36 hours. Convergence was monitored by usual trace plots (not shown), and the marginal and multivariate potential scale reduction factors (Brooks and Gelman (1998)).

Figure 3 shows a summary across quantiles for the fixed effects parameters and for ρ^τ, the mean of the spatial process $\rho^\tau(\mathbf{s})$. Figure S7 of the Supplementary Material provides the rest of the model parameters. As expected, β_0^τ increases monotonically with the quantiles, but it is not a linear function of τ since the slope varies from $\tau = 0.60$. The seasonal pattern obtained from the harmonic terms is very similar across the τ's. The elevation coefficient β_3^τ is close to $-7°$C/km, the environmental lapse rate (Navarro-Serrano et al. (2018)), for τ greater than or equal to 0.40. This value decreases below $-9°$C/km for τ's close to the extreme cold. The posterior median of α^τ is above 0.30°C/decade in the central quantiles, close to the trend of 0.27°C/decade estimated by Peña-Angulo et al. (2021) for the daily temperature in Spain in the summer period 1956–2015, and decreases to about 0.10°C/decade in the tails. The results of ρ^τ show a strong autoregression in all the quantiles, varying from 0.55 for $\tau = 0.05$ to 0.75 in the central quantiles.

Figure 4 shows the posterior mean of the spatial random effects, $\tilde{\beta}_0^\tau(\mathbf{s})$, $\tilde{\alpha}^\tau(\mathbf{s})$, $\rho^\tau(\mathbf{s})$, and $\sigma^\tau(\mathbf{s})$ at each observed site across quantiles. Figure 5 shows spatially the posterior mean of the previous spatial processes (showing $\beta_0^\tau(\mathbf{s})$ instead of $\tilde{\beta}_0^\tau(\mathbf{s})$) for $\tau = 0.05, 0.50, 0.95$. See also Figure S8 of the Supplementary Material for posterior boxplots of these processes at the observed sites and Figure S9 to get an idea of the uncertainties of these estimates. These figures show wide spatial variability in the four spatial processes at all quantiles. In particular,

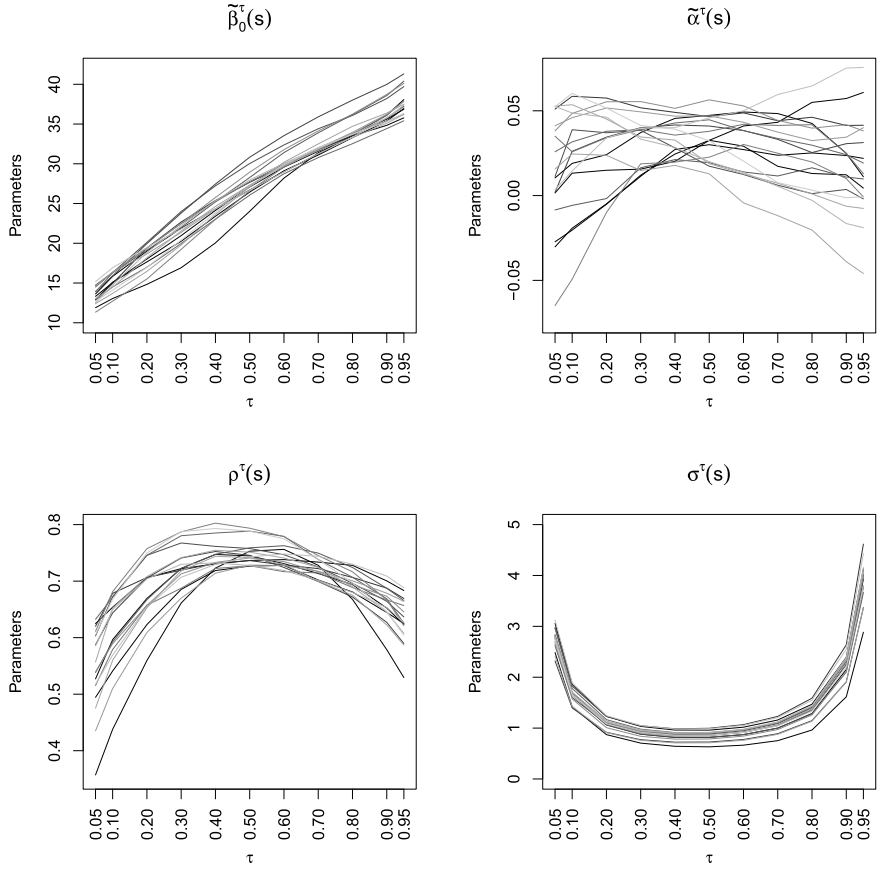

FIG. 4. *Posterior mean of the four spatial random effects in the* 18 *observed sites across quantiles*.

the spatially varying intercept $\beta_0^{\tau}(\mathbf{s})$ captures climate variability not explained by elevation. The similarity of the spatial pattern for $\beta_0^{0.50}(\mathbf{s})$ and $\beta_0^{0.95}(\mathbf{s})$ versus $\beta_0^{0.05}(\mathbf{s})$ is noteworthy. There are clear differences across quantiles in the spatial pattern of the linear trend $\tilde{\alpha}^{\tau}(\mathbf{s})$. For $\tau = 0.50$, the trends are positive in all of the regions while negative values are observed in the northwest for $\tau = 0.05$ and in the central part and northeast for $\tau = 0.95$. The areas where the 80% credible intervals do not contain a null trend are shown in Figure S10 of the Supplementary Material. The range and spatial pattern of the autoregression term $\rho^{\tau}(\mathbf{s})$ also vary across quantiles. The posterior mean varies from 0.72 to 0.80 in $\tau = 0.50$, from 0.53 to 0.69 in $\tau = 0.95$, and from 0.36 to 0.64 in $\tau = 0.05$.

The random evolution across years of the posterior distribution of the temporal random effects ψ_t^{τ} (see Figure S11 in the Supplementary Material) confirms that a more complex trend would not improve the fit of the linear trend. Again, we note the similarity of the distribution of $\psi_t^{0.50}$ and $\psi_t^{0.95}$, while $\psi_t^{0.05}$ is slightly different and has a greater variance.

3.3.1. *Conditional quantiles*. As an illustration of the output provided by the model, Figure 6 shows the posterior mean of the conditional quantiles $Q_{Y_{t\ell}(\mathbf{s})}(\tau \mid y)$ on July 15, 2015 ($t = 60$ and $\ell = 76$) under three different situations for y and for $\tau = 0.05, 0.50, 0.95$. An important feature of daily temperature is its high persistence, evidenced by the autoregression coefficients $\rho^{\tau}(\mathbf{s})$ of the model. The selected values of y correspond to location dependent cold, mild, and warm situations, that is, we use local empirical quantiles $q_{Y(\mathbf{s})}^{\text{emp}}(\tau^*)$ for $\tau^* = 0.05, 0.50, 0.95$. First, the empirical quantiles at the observed sites are obtained using the

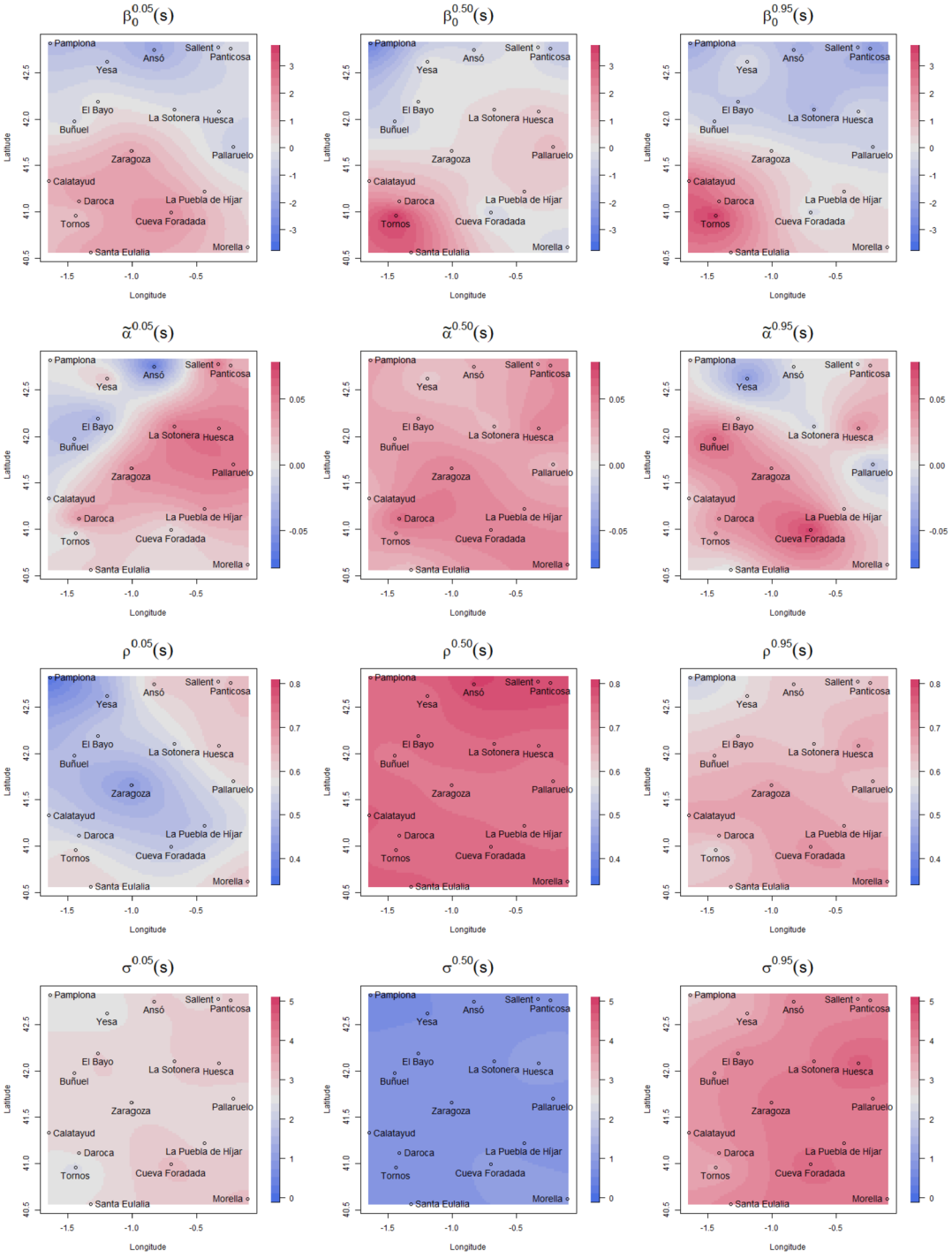

FIG. 5. *Maps of the posterior mean of the four spatial random effects for* $\tau = 0.05, 0.50, 0.95$.

30×92 observations of the JJA months in the reference period 1981–2010. Later, to obtain a value for each $\mathbf{s}$, the observed values are interpolated by means of a simple kriging.

Though the posterior mean level changes, the spatial pattern in all the conditional quantiles is similar. However, as a consequence of the different persistence across quantiles, the posterior mean of the difference between $Q_{Y_{t\ell}(\mathbf{s})}(0.50 \mid y)$ and $Q_{Y_{t\ell}(\mathbf{s})}(0.05 \mid y)$ varies noticeably depending on the value of the previous day's temperature. For example, in Zaragoza, it is

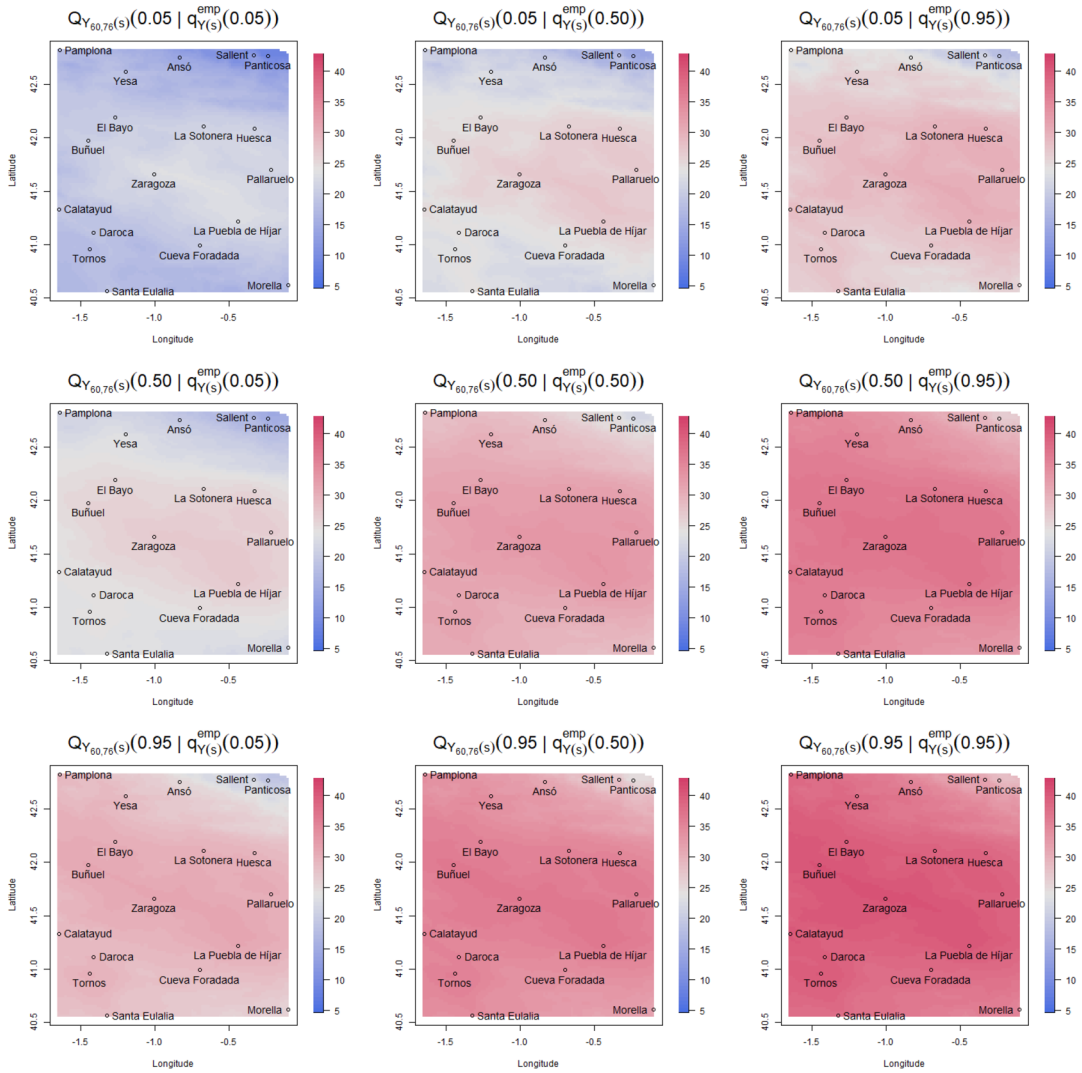

FIG. 6. *Maps of the posterior mean of the conditional quantiles* $Q_{Y_{60,76}(\mathbf{s})}(\tau \mid q^{\text{emp}}_{Y(\mathbf{s})}(\tau^*))$ *on July* 15, 2015, *for* $\tau, \tau^* = 0.05, 0.50, 0.95$.

2.8°C, 5.7°C and 8.6°C for $y = 20, 30, 40$°C, respectively. Analogously, the posterior mean of the difference between $Q_{Y_{t\ell}(\mathbf{s})}(0.95 \mid y)$ and $Q_{Y_{t\ell}(\mathbf{s})}(0.50 \mid y)$ is 4.3°C, 3.7°C, and 3.1°C for the previous values of y. Another consequence is that an increase of around 1°C in the previous day's temperature, y, yields an increase of around 0.44°C in the posterior mean of the 0.05 conditional quantile, 0.73°C in the conditional median, and around 0.66°C in the 0.95 conditional quantile.

3.4. *Model assessment through cross-validation.* Here, we take up model assessment in the context of performance across the n locations. That is, we are not implementing model comparison; rather, we are looking at local and global adequacy of the model employing three different quantiles, $\tau = 0.05, 0.50, 0.95$. In particular, a leave-one-out cross-validation is carried out. That is, each site is held out one at a time and subsequently the model is fitted with the remaining $n - 1$ sites. Then the conditional quantiles are obtained using one-step ahead prediction since, for held-out site, we know the $Y_{t,\ell-1}(\mathbf{s})$ to condition on.

We consider two types of residuals. The first type is defined as $R_{t\ell}^{(b)}(\tau;\mathbf{s}) = Y_{t\ell}(\mathbf{s}) - Q_{Y_{t\ell}(\mathbf{s})}^{(b)}(\tau \mid Y_{t,\ell-1}(\mathbf{s}))$ for $b = 1, 2, \ldots, B$, where b denotes an MCMC posterior realization of the τ conditional quantile on day ℓ, year t at site $\mathbf{s}$. A simpler type based on the mean of those realizations yields the single residual value $R_{t\ell}(\tau;\mathbf{s}) = Y_{t\ell}(\mathbf{s}) - E[Q_{Y_{t\ell}(\mathbf{s})}(\tau \mid Y_{t,\ell-1}(\mathbf{s})) \mid \text{data}]$. The simpler version only looks at $Y_{t\ell}(\mathbf{s})$ relative to the associated mean of the conditional quantile. The replicated version looks at $Y_{t\ell}(\mathbf{s})$ relative to the distribution of the associated conditional quantile.

Now, we define three measures of model assessment. First, we propose an approximation to the probability (an integral) that the observed $Y_{t\ell}(\mathbf{s})$ is less than the conditional quantile on day ℓ, year t, site $\mathbf{s}$. This probability is estimated as $p_{t\ell}(\tau;\mathbf{s}) = \sum_b \mathbf{1}(R_{t\ell}^{(b)}(\tau;\mathbf{s}) < 0)/B$. The mean value of these probabilities should be τ. As a result, a global measure is defined as

$$p(\tau) = \frac{1}{nT(L-1)} \sum_{i=1}^{n} \sum_{t=1}^{T} \sum_{\ell=2}^{L} p_{t\ell}(\tau;\mathbf{s}_i).$$

Under an adequate model, this should take a value close to τ. Analogous versions without averaging over days, years, or sites are denoted by $p_\ell(\tau)$, $p_t(\tau)$, or $p(\tau;\mathbf{s})$, respectively.

Second, to evaluate potential overfit in terms of out of sample performance, we employ the asymmetrically τ-weighted mean absolute error (Koenker and Bassett (1978)), which we denote by WMAE(τ). Using the check loss function $\delta_\tau(u) = u(\tau - \mathbf{1}(u < 0))$ defined in Section 3.1, this measure is given by

$$\text{WMAE}(\tau) = \frac{1}{nT(L-1)} \sum_{i=1}^{n} \sum_{t=1}^{T} \sum_{\ell=2}^{L} \delta_\tau\big(R_{t\ell}(\tau;\mathbf{s}_i)\big).$$

Equivalently, this measure calculates the mean value of the absolute errors weighted by $1-\tau$ if $R_{t\ell}(\tau;\mathbf{s}) < 0$ or τ otherwise. The smaller its value, the better the model performance. The analogous site-level version is denoted by WMAE($\tau;\mathbf{s}$).

The third measure is calculated as $R^1(\tau)$ according to Koenker and Machado (1999). This goodness-of-fit measure is viewed as an analogue of R^2 for the classical residual sum of squares; the check loss function for quantiles replaces the least-squares loss function and the τ empirical quantile $q_{Y(\mathbf{s})}^{\text{emp}}(\tau)$ replaces the sample mean. In this section, $q_{Y(\mathbf{s})}^{\text{emp}}(\tau)$ is calculated with the $T \times (L-1)$ observations of the held-out site. Thus, this measure is given by

$$R^1(\tau) = 1 - \frac{\sum_{i=1}^{n} \sum_{t=1}^{T} \sum_{\ell=2}^{L} \delta_\tau(R_{t\ell}(\tau;\mathbf{s}_i))}{\sum_{i=1}^{n} \sum_{t=1}^{T} \sum_{\ell=2}^{L} \delta_\tau(Y_{t\ell}(\mathbf{s}_i) - q_{Y(\mathbf{s}_i)}^{\text{emp}}(\tau))}.$$

Note that in-sample, but not out-of-sample, $R^1(\tau)$ would fall between 0 and 1. In both cases, it measures the relative success of the corresponding QR models at a specific quantile in terms of an appropriately weighted sum of absolute residuals. Thus, $R^1(\tau)$ provides a local measure of goodness-of-fit for a particular quantile rather than a global measure of goodness-of-fit over the entire conditional distribution. The analogous site-level version is denoted by $R^1(\tau;\mathbf{s})$.

Table 1 shows global performance metrics and Table 2 shows the results by site. The performance is good for the three values of τ according to $p(\tau)$. Further, for most of the stations, $p(\tau;\mathbf{s})$ is within $\tau \pm 0.02$. The goodness-of-fit considering $R^1(\tau)$ is around 0.367 for $\tau = 0.05$, with values above 0.4 in some sites. This criteria is around 0.464 and 0.442 for $\tau = 0.50$ and 0.95, respectively, but it is above 0.5 in some sites. Quantiles 0.50 and 0.95 perform better than the left tail.

TABLE 1
Performance metrics for the models with $\tau = 0.05, 0.50, 0.95$

τ	$p(\tau)$	WMAE(τ)	$R^1(\tau)$
0.05	0.056	0.378	0.367
0.50	0.505	1.192	0.464
0.95	0.944	0.272	0.442

Less accurate results appear in sites located in the western part of the region. Tornos has a climate that is affected by plateau conditions, and presents the worst values in $p(\tau; \mathbf{s})$ and $R^1(\tau; \mathbf{s})$ for $\tau = 0.95$. Pamplona has colder conditions related to Cantabrian Sea effects, and the actual $\tau = 0.05$ quantile is much colder than expected by the model. Furthermore, its median is the most poorly captured across the sites. The performance of the other sites is reasonably homogeneous based on the three measures for the three values of τ.

Figure 7 shows the evolution of $p_t(\tau)$ and $p_\ell(\tau)$ across t and ℓ, respectively. It reveals that the temporal evolution of days-within-years and years is well captured and there seems to be no bias in the estimates.

4. Marginal quantiles. Here, we present a general strategy for obtaining marginal quantiles from the conditional quantiles. Implementation is straightforward working with AL errors, employing the conditional Gaussian representation.

Marginal quantiles enjoy direct interpretation as well as the benefit of spatial interpolation. That is, to be locally appropriate, conditional quantiles would require the local previous day's temperature, which will not be available at unobserved locations.[2] We present the approach

TABLE 2
Performance metrics for models with $\tau = 0.05, 0.50, 0.95$ *for the* 18 *sites*

	$p(\tau; \mathbf{s})$			WMAE($\tau; \mathbf{s}$)			$R^1(\tau; \mathbf{s})$		
Location	0.05	0.50	0.95	0.05	0.50	0.95	0.05	0.50	0.95
Pamplona	0.140	0.582	0.933	0.501	1.619	0.359	0.144	0.333	0.369
Buñuel	0.069	0.519	0.954	0.368	1.227	0.270	0.345	0.422	0.430
El Bayo	0.036	0.485	0.952	0.367	1.162	0.262	0.361	0.457	0.444
Morella	0.035	0.531	0.953	0.342	1.046	0.250	0.418	0.488	0.460
Huesca	0.040	0.485	0.954	0.341	1.005	0.225	0.398	0.520	0.515
Tornos	0.051	0.446	0.876	0.436	1.392	0.349	0.386	0.458	0.347
Santa Eulalia	0.037	0.463	0.951	0.390	1.137	0.257	0.393	0.510	0.480
Calatayud	0.044	0.504	0.944	0.372	1.221	0.279	0.411	0.473	0.451
Panticosa	0.042	0.568	0.976	0.346	1.110	0.267	0.402	0.491	0.419
La Puebla de Híjar	0.063	0.465	0.925	0.377	1.118	0.252	0.342	0.462	0.449
Ansó	0.045	0.524	0.969	0.370	1.160	0.262	0.392	0.490	0.463
Daroca	0.053	0.523	0.968	0.380	1.275	0.274	0.394	0.454	0.456
Zaragoza	0.066	0.505	0.957	0.365	1.176	0.244	0.350	0.446	0.484
La Sotonera	0.055	0.506	0.941	0.361	1.094	0.251	0.378	0.493	0.470
Pallaruelo	0.058	0.481	0.932	0.373	1.106	0.250	0.375	0.488	0.463
Cueva Foradada	0.046	0.573	0.976	0.326	1.027	0.246	0.396	0.477	0.452
Sallent de Gállego	0.060	0.465	0.914	0.373	1.167	0.276	0.389	0.487	0.429
Yesa	0.062	0.464	0.910	0.423	1.414	0.316	0.324	0.416	0.411

[2]Of course, we can always interpolate conditional quantiles given illustrative choices of previous day's temperature.

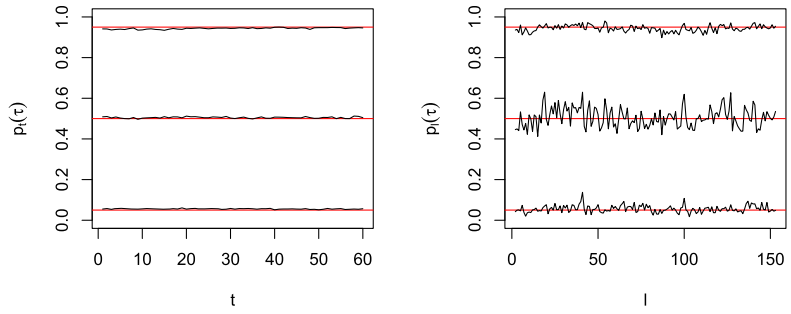

FIG. 7. *Evolution of $p_t(\tau)$ across t (left) and $p_\ell(\tau)$ across ℓ (right) for $\tau = 0.05, 0.50, 0.95$.*

for extracting a marginal quantile from a conditional quantile *after* fitting the conditional quantile model. In the setting of an AL specification for the errors, first we show how to implement this procedure for a single day. Next, we clarify how the spatial kriging is implemented using these marginal quantiles and supply a spatial map of the marginal τ-quantile temperature surface in our study region for a given day. Then we move to the marginal quantile associated with an average over days. Such averaging is helpful in providing say, weekly quantiles; in our application, 7-day average temperatures quantiles in the summer may be useful, particularly for comparison over years. Such quantiles can be kriged over a spatial region to reveal the *quantile surface*. Lastly, such a daily or weekly quantile surface can be averaged over a region of interest to obtain areal daily or weekly quantiles. The tool here is block averaging (Banerjee, Carlin and Gelfand (2015), Chapter 7).

4.1. *Obtaining marginal quantiles from conditional quantiles in an autoregression.* Considering expression (2), it is attractive to think about $q^\tau_{t\ell}(\mathbf{s})$ as a version of a marginal τ quantile for $Y_{t\ell}(\mathbf{s})$. However, $P(Y_{t\ell}(\mathbf{s}) \le q^\tau_{t\ell}(\mathbf{s})) \ne \tau$. So, we seek an additive adjustment to $q^\tau_{t\ell}(\mathbf{s})$, which depends upon the model for $Y_{t\ell}(\mathbf{s})$, so that it adjusts this probability to τ. Then $q^\tau_{t\ell}(\mathbf{s})$ plus this adjustment becomes the marginal τ quantile we want.

To present the idea in its simplest form, we ignore space and years and suppress the superscript τ in the parameters. So, we have $Y_\ell = q_\ell + \rho(Y_{\ell-1} - q_{\ell-1}) + \epsilon_\ell$ where the $\epsilon_\ell \sim$ i.i.d. AL$(0, \sigma, \tau)$. In this notation, $Q_{Y_\ell}(\tau \mid Y_{\ell-1}) = q_\ell + \rho(Y_{\ell-1} - q_{\ell-1})$ is the τ quantile of the QAR. For convenience, write this model as $W_\ell = \rho W_{\ell-1} + \epsilon_\ell$ with $W_\ell = Y_\ell - q_\ell$. Upon substitution, we have $W_\ell = \rho^\ell W_0 + \sum_j \rho^j \epsilon_{\ell-j}$. Using the conditional normal form for ϵ_ℓ in (1), we have

$$\tilde{\epsilon}_\ell \mid \rho, \sigma, U_\ell, U_{\ell-1}, \ldots, U_1 \equiv \sum_{j=0}^{\ell-1} \rho^j \epsilon_{\ell-j} \mid \rho, \sigma, U_\ell, U_{\ell-1}, \ldots, U_1$$
$$\sim N\left(\frac{1-2\tau}{\sigma\tau(1-\tau)} \sum_{j=0}^{\ell-1} \rho^j U_{\ell-j}, \frac{2}{\sigma^2\tau(1-\tau)} \sum_{j=0}^{\ell-1} \rho^{2j} U_{\ell-j} \right).$$

We want the τ quantile of W_ℓ, call it $d^\tau_\ell(\rho, \sigma)$, so that $W_\ell - d^\tau_\ell(\rho, \sigma)$ has 0 as its τ quantile and, therefore, Y_ℓ has $q_\ell + d^\tau_\ell(\rho, \sigma)$ as the τ marginal quantile. The τ quantile of W_ℓ is $\rho^\ell W_0$ plus the τ quantile of $\tilde{\epsilon}_\ell$. While 0 is the τ quantile of ϵ_ℓ, the τ quantile of $\tilde{\epsilon}_\ell$ will not be 0. That is, each term in $\tilde{\epsilon}_\ell$ has τ quantile 0 but the sum will not.

Though $\tilde{\epsilon}_\ell$ does not have an AL distribution, we can find its τ quantile. For any d, we seek $P(\tilde{\epsilon}_\ell < d \mid \rho, \sigma)$. However,

$$P(\tilde{\epsilon}_\ell < d \mid \rho, \sigma)$$
$$= \int\int \cdots \int P(\tilde{\epsilon}_\ell < d \mid \rho, \sigma, \{U_j : j = 1, 2, \ldots, \ell\}) [\{U_j\}] \, dU_1 \, dU_2 \cdots dU_\ell.$$

But given $\{U_j : j = 1, 2, \ldots, \ell\}$, we have the distribution for $\tilde{\epsilon}_\ell$ above. So, we can calculate $P(\tilde{\epsilon}_\ell < d \mid \rho, \sigma, \{U_j : j = 1, 2, \ldots, \ell\})$. In fact, we can do a Monte Carlo integration to calculate $P(\tilde{\epsilon}_\ell < d \mid \rho, \sigma)$ by generating many sets $\{U_j : j = 1, 2, \ldots, \ell\}$, all i.i.d., all distributed as Exp(1). We can do this for any value d, in fact, using the same Monte Carlo samples. Then, using a simple search, we can find $d_\ell^\tau(\rho, \sigma)$. Moreover, we can use the same Monte Carlo samples for any ρ and σ so computation is not demanding.

In our modeling setting, we need $d_{t\ell}^\tau(\rho^\tau(\mathbf{s}), \sigma^\tau(\mathbf{s}))$ to accompany $q_{t\ell}^\tau(\mathbf{s})$. From the model fitting described in Section 3.2.1, we have random samples of $\rho^\tau(\mathbf{s})$ and $\sigma^\tau(\mathbf{s})$, which can produce random samples of $d_{t\ell}^\tau(\rho^\tau(\mathbf{s}), \sigma^\tau(\mathbf{s}))$. These can be used with posterior samples of $q_{t\ell}^\tau(\mathbf{s})$ to create the posterior distribution of the τ marginal quantile for any year, day, and site. In the sequel, we denote this as $\tilde{q}_{Y_{t\ell}(\mathbf{s})}(\tau) \equiv q_{t\ell}^\tau(\mathbf{s}) + d_{t\ell}^\tau(\rho^\tau(\mathbf{s}), \sigma^\tau(\mathbf{s}))$. Again, we can use the same sets of $\{U_j\}$'s. Moreover, we can do this for any τ. Generating the entire collection of marginal quantiles of interest is straightforward.

4.2. *Kriging marginal quantiles and block averaging of marginal spatial quantiles.* As above, for a given τ, year, and day within year, marginal quantiles enable kriging to unobserved locations. More precisely, at new site $\mathbf{s}_0$, we can obtain the posterior distribution of $\tilde{q}_{Y_{t\ell}(\mathbf{s}_0)}(\tau)$. To obtain a sample of $\tilde{q}_{Y_{t\ell}(\mathbf{s}_0)}(\tau)$, we need a sample of the model part plus a sample of the adjustment part, $d_{t\ell}^\tau(\rho^\tau(\mathbf{s}_0), \sigma^\tau(\mathbf{s}_0))$. The model part is a function of the parameters and process realizations while the correction part is a function of just process realizations. Posterior samples for the parameters are available from the model fitting. Posterior samples for the GPs are available, using posterior samples of the parameters, through usual Bayesian kriging (Banerjee, Carlin and Gelfand (2015), Chapter 6). Therefore, we can interpolate marginal quantiles to any desired location in the study region. If we do this to a sufficiently spatially resolved grid, we can obtain the posterior mean at each point and "see" the posterior τ quantile surface for the given day within year.

Further, we might seek the average of the τ quantile over some subregion $\mathcal{B} \subseteq \mathcal{D}$ for day ℓ in year t. This becomes a block average, $\tilde{q}_{Y_{t\ell}(\mathcal{B})}(\tau) \equiv \int_{\mathcal{B}} \tilde{q}_{Y_{t\ell}(\mathbf{s})}(\tau)\, d\mathbf{s}/|\mathcal{B}|$. As is customary, we approximate this integral by Monte Carlo integration of the form $\sum_{k=1}^K \tilde{q}_{Y_{t\ell}(\mathbf{s}_k)}(\tau)/K$ for $\{\mathbf{s}_k \in \mathcal{B}\}$, drawing the $\mathbf{s}_k$ from above grid. Lastly, we note that in the above, we are interpolating a parameter, not an observation. We are obtaining posterior distributions, not posterior predictive distributions.

4.2.1. *Marginal quantiles for one day at unobserved locations.* For each of the 3000 posterior samples of $\rho^\tau(\mathbf{s}_i)$ and $\sigma^\tau(\mathbf{s}_i)$ $(i = 1, \ldots, n)$ stored in Section 3.3, we use Bayesian kriging to obtain 3000 samples of $\rho^\tau(\mathbf{s}_k)$ and $\sigma^\tau(\mathbf{s}_k)$ $(k = 1, \ldots, K)$ in a grid of the study region $\mathcal{D}$ (see Section 2 for grid details). For each of them, we sample 1000 sets of $\{U_j\}$'s to calculate $P(\tilde{\epsilon}_\ell < d \mid \rho, \sigma)$, and obtain a sample of $d_{t\ell}^\tau(\rho^\tau(\mathbf{s}_k), \sigma^\tau(\mathbf{s}_k))$ through a one-dimensional rootfinder. In particular, $\rho^\ell W_0$ drops rapidly to zero as ℓ tends to infinity, so it becomes negligible.

As an illustration of the output provided by the marginal quantiles, Figure 8 shows maps of the posterior mean of $\tilde{q}_{Y_{t\ell}(\mathbf{s})}(\tau)$ on July 15, 2015 ($t = 60$ and $\ell = 76$) for $\tau = 0.05, 0.50, 0.95$. For all quantiles, the maximum temperature is reached in the Valley, center and southeast, and the minimum in the Pyrenees in the northeast. For $\tau = 0.05$, the temperature range goes from 6.0°C to 27.9°C, for $\tau = 0.50$ from 19.7°C to 37.1°C, and for $\tau = 0.95$ from 23.3°C to 41.1°C.

We use the marginal quantiles to analyze climate change for $\tau = 0.05, 0.50, 0.95$ in Figure 9. The first row shows spatially

$$E\Bigg(\frac{1}{10}\sum_{t \in D6} \tilde{q}_{Y_{t\ell}(\mathbf{s})}(\tau) - \frac{1}{10}\sum_{t' \in D1} \tilde{q}_{Y_{t'\ell}(\mathbf{s})}(\tau) \,\Big|\, \text{data}\Bigg), \tag{3}$$

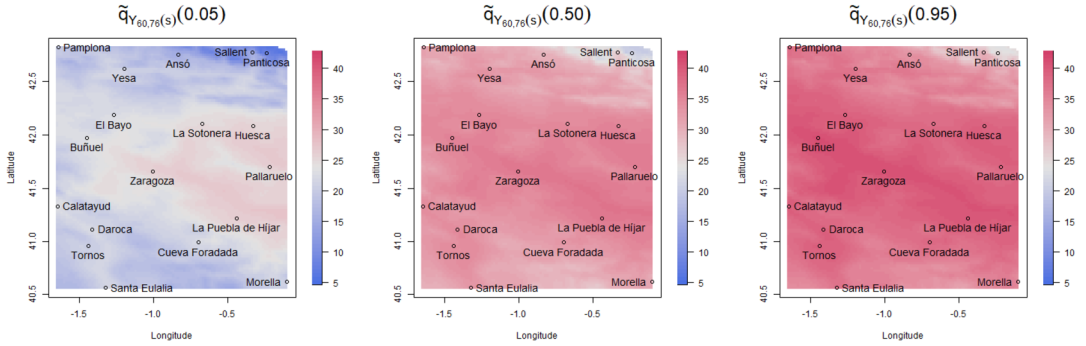

FIG. 8. *Maps of the posterior mean of the marginal quantiles* $\tilde{q}_{Y_{60,76}(\mathbf{s})}(\tau)$ *on July* 15, 2015, *for* $\tau = 0.05, 0.50, 0.95$.

where $D1$ is the first decade (1956–1965) and $D6$ the last (2006–2015). The result does not depend on ℓ since it can be summed up to the change in the terms $\alpha^\tau t + \gamma_t^\tau(\mathbf{s})$. The posterior mean in (3) supplies the mean change in temperature between the marginal quantile of a day averaged over the first decade and the marginal quantile of that same day averaged over the last decade, that is, we use averages of daily quantiles. The spatial pattern appears different across quantiles, with a smaller range of change for the median than for the extreme quantiles. Warming is general, exceeding 3°C in the southwest for $\tau = 0.95$. But cooling patterns also appear in the northwest for $\tau = 0.05$.

The second row shows spatially

$$P\big(\tilde{q}_{Y_{t'\ell}(\mathbf{s})}(\tau) < \tilde{q}_{Y_{t\ell}(\mathbf{s})}(\tau) \mid t' \in D1, t \in D6, \text{data}\big). \tag{4}$$

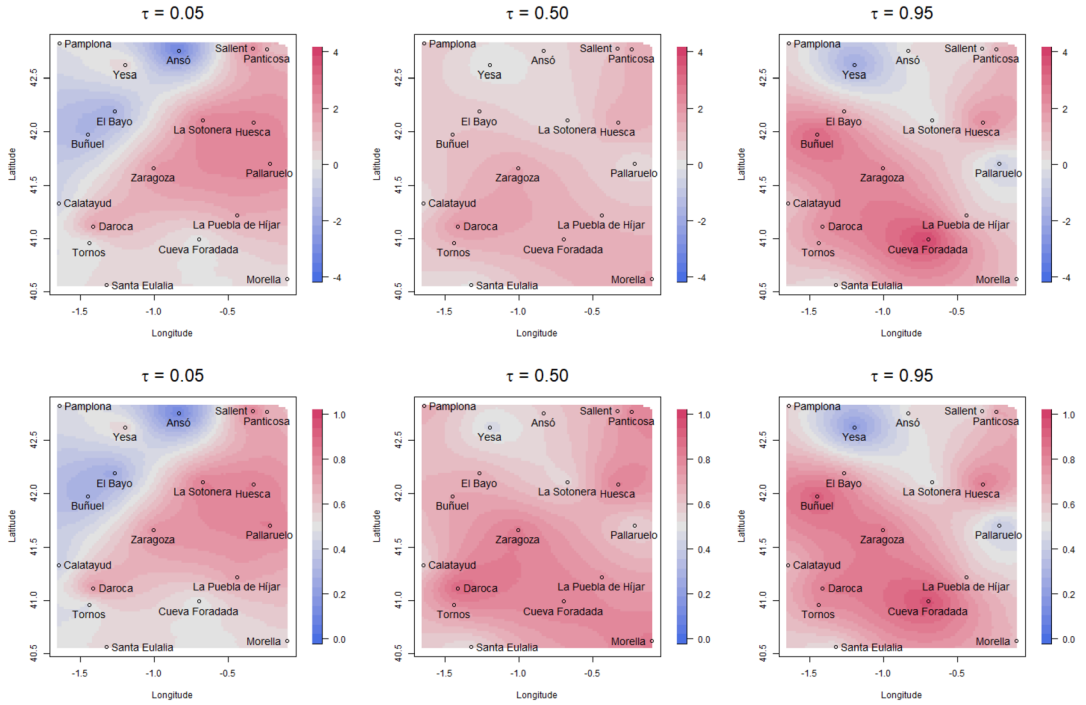

FIG. 9. *Top*: *Difference* (*in* °*C*) *between the marginal quantiles of the last and the first decades in* (3). *Bottom*: *Posterior probability in* (4) *that a marginal quantile in a day in a year of the first decade is colder than the same day in a year of the last decade. For* $\tau = 0.05, 0.50, 0.95$.

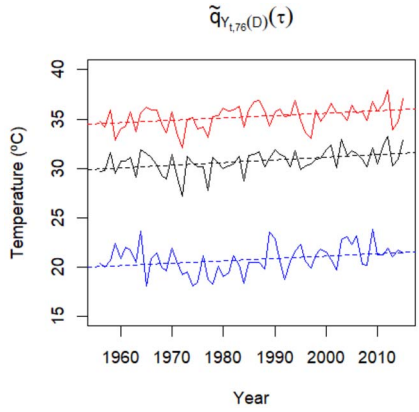

FIG. 10. *Evolution of the block average* $\tilde{q}_{Y_{t,76}(\mathcal{D})}(\tau)$ *on July* 15 *against year for* $\tau = 0.05, 0.50, 0.95$.

This value represents the posterior probability that the marginal quantile of a day in any year of the first decade is colder than the marginal quantile of that same day for any year of the last decade. The pattern is the same as above, but in this case instead of seeing results in °C, we see them in terms of probabilities. To summarize the results, if we also condition on $\mathbf{s} \in \mathcal{D}$ in (4), these posterior probabilities are 0.67 for $\tau = 0.50$, 0.66 for $\tau = 0.95$, and 0.57 for $\tau = 0.05$.

Figure 10 shows the evolution over the years of the block average $\tilde{q}_{Y_{t\ell}(\mathcal{D})}(\tau)$ for July 15 ($\ell = 76$). A warming trend is observed in all three quantiles. Although the baseline may change for other choices of ℓ, the pattern through the years will be common.

4.3. *Marginal quantiles for averages.* Next, we take up averaging over time to obtain say, a weekly τ quantile at site $\mathbf{s}$ in year t. To simplify notation, we suppress the year, the site, and the superscript τ. Suppose we want to average back r days, starting at day $\ell \geq r$. So, we are seeking the marginal τ-quantile of $\bar{Y}_\ell^{(r)} = \frac{1}{r}\sum_{j=\ell-r+1}^{\ell} Y_j$. To be clear, we want the quantile of this average, not the average of the daily quantiles. Going one step further, if we want to average over space (as above) and time, we should first average over time and then average over space. That is, the quantile of the temporal average is not the average of the temporal quantiles but $\tilde{q}_{Y_{t\ell}(\mathcal{B})}(\tau)$, by definition, is an average of quantiles.

From above, we have $Y_\ell = q_\ell + \rho(Y_{\ell-1} - q_{\ell-1}) + \epsilon_\ell$ where the $\epsilon_\ell \sim$ i.i.d. AL$(0, \sigma, \tau)$. So, again, $Q_{Y_\ell}(\tau \mid Y_{\ell-1}) = q_\ell + \rho(Y_{\ell-1} - q_{\ell-1})$ is the τ quantile for the QAR for day ℓ. Again, for convenience, write this model as $W_\ell = \rho W_{\ell-1} + \epsilon_\ell$ with $W_\ell = Y_\ell - q_\ell$.

Then, if $\bar{W}_\ell^{(r)} = \frac{1}{r}\sum_{j=\ell-r+1}^{\ell} W_j$, $\bar{W}_\ell^{(r)} = \bar{Y}_\ell^{(r)} - \bar{q}_\ell^{(r)}$ where $\bar{q}_\ell^{(r)}$ averages the q's accordingly. So, the marginal τ quantile for $\bar{Y}_\ell^{(r)}$ will be $\bar{q}_\ell^{(r)}$ plus an adjustment.

Since $W_j = \rho^j W_0 + \sum_{k=0}^{j-1} \rho^k \epsilon_{j-k}$, we need the τ quantile of

$$\bar{\bar{\epsilon}}_\ell^{(r)} \equiv \frac{1}{r} \sum_{j=\ell-r+1}^{\ell} \sum_{k=0}^{j-1} \rho^k \epsilon_{j-k}.$$

Note that, while the double sum is over $r(\ell-r)+r(r+1)/2$ terms, it only involves $\epsilon_1, \ldots, \epsilon_\ell$. We can rewrite the sum in terms of these ℓ distinct ϵ's but to no advantage. Rather, we need to generate ℓ associated U's, that is, ℓ i.i.d. Exp(1) random variables. For each ρ, σ, and given these U's,

$$\bar{\bar{\epsilon}}_\ell^{(r)} \sim N\left(\frac{1-2\tau}{\sigma\tau(1-\tau)}\frac{1}{r}\sum_{j=\ell-r+1}^{\ell}\sum_{k=0}^{j-1}\rho^k U_{j-k}, \frac{2}{\sigma^2\tau(1-\tau)}\frac{1}{r^2}\sum_{j=\ell-r+1}^{\ell}\sum_{k=0}^{j-1}\rho^{2k}U_{j-k}\right).$$

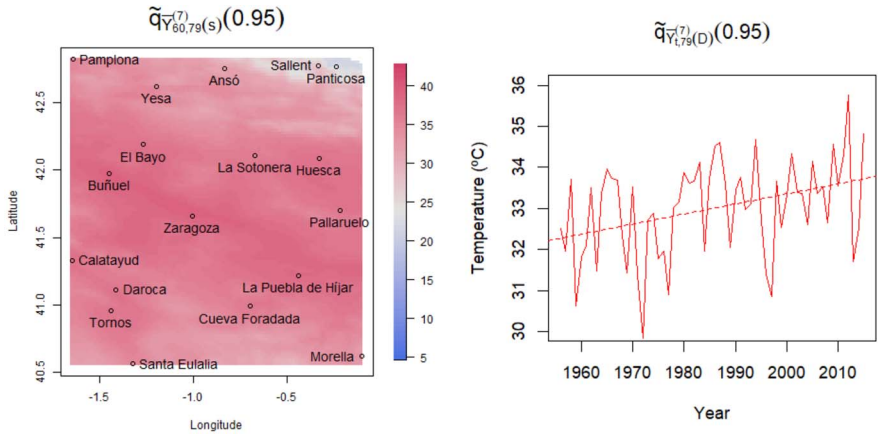

FIG. 11. *Left*: *Map of the posterior mean of the weekly marginal quantiles* $\tilde{q}_{\bar{Y}^{(7)}_{60,79}(\mathbf{s})}(0.95)$ *centered on July* 15, 2015. *Right*: *Evolution of the block average of the weekly marginal quantiles* $\tilde{q}_{\bar{Y}^{(7)}_{t,79}(\mathcal{D})}(0.95)$ *centered on July* 15 *against year.*

Again, using a simple search, we can find the τ quantile of $\bar{\tilde{\epsilon}}^{(r)}_{\ell}$ and, therefore, we can find the adjustment to obtain the τ marginal quantile for $\bar{Y}^{(r)}_{\ell}$. In our modeling setting, we denote this quantile by $\tilde{q}_{\bar{Y}^{(r)}_{t\ell}(\mathbf{s})}(\tau)$. With posterior samples from the model fitting, we can create a posterior distribution for this marginal quantile. We can do this for any location, averaging back from any day within a year, and for any year. Thus, we can create an associated spatial surface. Note that we can reuse the U's except the number that we require depends upon ℓ as above. Finally, if we want this τ marginal quantile averaged over a region say, $\mathcal{B}$, we can implement an analogous Monte Carlo integration as above, replacing $\tilde{q}_{Y_{t\ell}(\mathbf{s})}(\tau)$ with $\tilde{q}_{\bar{Y}^{(r)}_{t\ell}(\mathbf{s})}(\tau)$.

4.3.1. *Weekly marginal quantiles at a given site.* Note that in climate analysis some extreme events are defined by the integration of the temperature series over several days. For example, Cattiaux and Ribes (2018) study the probability of extremely hot temperatures during a moving-window of $r = 2, 3, \ldots, 15$ days in Paris, and Lee (2021) analyzes trends in extreme "weather whiplash" events defined by daily temperature in a 7-day moving window. Here, as an example of application of the proposed methodology, we follow the setup in Section 4.2.1 to obtain weekly marginal quantiles $\tilde{q}_{\bar{Y}^{(r)}_{t\ell}(\mathbf{s})}(\tau)$ centered at July 15, 2015 ($t = 60$, $\ell = 79$ and $r = 7$), for $\tau = 0.95$.

In particular, the plot on the left of Figure 11 shows the map of the posterior mean of $\tilde{q}_{\bar{Y}^{(r)}_{t\ell}(\mathbf{s})}(\tau)$ centered on July 15, 2015 ($t = 60$, $\ell = 79$ and $r = 7$) for $\tau = 0.95$. The spatial pattern is the same as for the daily marginal quantiles, but the temperature range is 21.2–38.9°C. The plot on the right of Figure 11 shows the weekly block average centered on July 15 across years for $\tau = 0.95$.

Lastly, other values of r can be considered but, if r is taken too large, many values will be averaged and, therefore, the quantiles from this averaging will get closer and closer. This can cause quantile crossing even for quantiles that are far from each other.

5. Summary and future work. This paper develops a modeling approach to predict a specific quantile in a spatiotemporal framework. We have specified a spatial conditional autoregressive model on a daily scale using the AL distribution for the errors. The considered specification enables spatial autoregression at a daily scale that captures serial correlation and facilitates assessment of persistence. The flexibility of the model is increased by considering

two scales of time—days within summer season and years—as well as seasonal behavior, time trend, and four GPs that represent the spatial dependence of the intercept, the trend, the serial dependence, and the scale of the AL errors. Bayesian model fitting enables full posterior inference for a given quantile. Although the model gives conditional quantiles, we offer an attractive approach to obtain marginal quantiles at daily scale. These marginal quantiles enable interpolation. The approach can also provide marginal quantiles associated with averages of the response variable, both spatially and dynamically. Posterior inference to evaluate changes between marginal quantiles of spatial and time averages can also be implemented.

The suggested QAR modeling approach is shown to be flexible enough to represent the evolution of different quantiles of the distribution of daily maximum temperatures and to capture the effects of climate change during the period 1956–2015 in Aragón, a small region but with a wide variety of climate conditions. The strong serial correlation of daily temperature is adequately captured by the autoregressive structure. The elevation, the only spatial covariate in the model, together with the four considered GPs are able to capture the great variability in climate conditions over the region; in particular, they capture observed features of temperature by allowing mean levels, trends over time, and serial correlation of temperature to vary spatially. The QAR models fitted for $\tau = 0.05, 0.50, 0.95$ show different spatial and temporal patterns, revealing important differences in the behavior of the tails versus the central part of the distribution of daily temperature in summer. More precisely, comparing the increases over time observed in the median, the 0.95 quantile shows higher increases in some areas of the Valley, while for the 0.05 quantile, no increase is observed in the northwest. These differences confirm the importance of modeling the entire distribution of daily temperature, rather than just the mean (as done in many climate studies). A useful climate application of the proposed methodology to estimate quantiles is the computation of thresholds to define extreme indexes or extreme events, taking into account changes over time of temperature.

Future work will consider different spatial regions providing more spatial sites than our sparse Aragón data set. This will enable comparison of temperature trends at larger spatial scales. Additionally, our modeling approach could be useful in other environmental analyses such as pollution exposure or biological experimental data, where the objective is to identify distributional changes over time and compare these changes across different spatial locations. Further, though the proposed modeling analyzes daily series across years, the approach could be applied to other time scales.

Acknowledgments. This work was done in part while J. C.-M. was a Visiting Scholar at the Department of Statistical Science from Duke University. The authors thank AEMET for providing the data. The authors are grateful to the Editor, the Associate Editor, and two reviewers for their insightful and constructive remarks on an earlier version of the paper.

Funding. This work was partially supported by the Grant PID2020-116873GB-I00 funded by MCIN/AEI/10.13039/501100011033; the Research Group E46_20R: Modelos Estocásticos funded by Gobierno de Aragón; and J. C.-M. was supported by the Doctoral Scholarship ORDEN CUS/581/2020 funded by Gobierno de Aragón.

SUPPLEMENTARY MATERIAL

Supplement to "Spatial quantile autoregression for season within year daily maximum temperature data" (DOI: 10.1214/22-AOAS1719SUPP; .pdf). This Supplementary Material provides additional details for the descriptive data analysis, a residual analysis, the details of the Gibbs sampler algorithm used to fit the model, and additional figures for the results of model fitting.

REFERENCES

AEMET (2011). Atlas Climático Ibérico—Iberian Climate Atlas. Ministerio de Medio Ambiente, y Medio Rural y Marino; Agencia Estatal de Meteorología; and Instituto de Meteorologia de Portugal. https://doi.org/10.31978/784-11-002-5

BANERJEE, S., CARLIN, B. P. and GELFAND, A. E. (2015). *Hierarchical Modeling and Analysis for Spatial Data*, 2nd ed. *Monographs on Statistics and Applied Probability* **135**. CRC Press, Boca Raton, FL. MR3362184 https://doi.org/10.1201/b17115

BROOKS, S. P. and GELMAN, A. (1998). General methods for monitoring convergence of iterative simulations. *J. Comput. Graph. Statist.* **7** 434–455. MR1665662 https://doi.org/10.2307/1390675

CASTILLO-MATEO, J., LAFUENTE, M., ASÍN, J., CEBRIÁN, A. C., GELFAND, A. E. and ABAURREA, J. (2022). Spatial modeling of day-within-year temperature time series: An examination of daily maximum temperatures in Aragón, Spain. *J. Agric. Biol. Environ. Stat.* **27** 487–505. MR4459077 https://doi.org/10.1007/s13253-022-00493-3

CASTILLO-MATEO, J., ASÍN, J., CEBRIÁN, A. C., GELFAND, A. E. and ABAURREA, J. (2023). Supplement to "Spatial quantile autoregression for season within year daily maximum temperature data." https://doi.org/10.1214/22-AOAS1719SUPP

CATTIAUX, J. and RIBES, A. (2018). Defining single extreme weather events in a climate perspective. *Bull. Am. Meteorol. Soc.* **99** 1557–1568. https://doi.org/10.1175/BAMS-D-17-0281.1

CHEN, X. and TOKDAR, S. T. (2021). Joint quantile regression for spatial data. *J. R. Stat. Soc. Ser. B. Stat. Methodol.* **83** 826–852. MR4320003 https://doi.org/10.1111/rssb.12467

CHERNOZHUKOV, V. and HONG, H. (2003). An MCMC approach to classical estimation. *J. Econometrics* **115** 293–346. MR1984779 https://doi.org/10.1016/S0304-4076(03)00100-3

DAS, P. and GHOSAL, S. (2017a). Bayesian quantile regression using random B-spline series prior. *Comput. Statist. Data Anal.* **109** 121–143. MR3603645 https://doi.org/10.1016/j.csda.2016.11.014

DAS, P. and GHOSAL, S. (2017b). Analyzing ozone concentration by Bayesian spatio-temoral quantile regression. *Environmetrics* **28** e2443, 15 pp. MR3660099 https://doi.org/10.1002/env.2443

GAO, M. and FRANZKE, C. L. E. (2017). Quantile regression-based spatiotemporal analysis of extreme temperature change in China. *J. Climate* **30** 9897–9914. https://doi.org/10.1175/JCLI-D-17-0356.1

GELFAND, A. E., SAHU, S. K. and CARLIN, B. P. (1995). Efficient parameterisations for normal linear mixed models. *Biometrika* **82** 479–488. MR1366275 https://doi.org/10.1093/biomet/82.3.479

HALLIN, M., LU, Z. and YU, K. (2009). Local linear spatial quantile regression. *Bernoulli* **15** 659–686. MR2555194 https://doi.org/10.3150/08-BEJ168

HAUGEN, M. A., STEIN, M. L., MOYER, E. J. and SRIVER, R. L. (2018). Estimating changes in temperature distributions in a large ensemble of climate simulations using quantile regression. *J. Climate* **31** 8573–8588. https://doi.org/10.1175/JCLI-D-17-0782.1

KOENKER, R. (2005). *Quantile Regression*. *Econometric Society Monographs* **38**. Cambridge Univ. Press, Cambridge. MR2268657 https://doi.org/10.1017/CBO9780511754098

KOENKER, R. and BASSETT, G. JR. (1978). Regression quantiles. *Econometrica* **46** 33–50. MR0474644 https://doi.org/10.2307/1913643

KOENKER, R. and MACHADO, J. A. F. (1999). Goodness of fit and related inference processes for quantile regression. *J. Amer. Statist. Assoc.* **94** 1296–1310. MR1731491 https://doi.org/10.2307/2669943

KOENKER, R. and XIAO, Z. (2006). Quantile autoregression. *J. Amer. Statist. Assoc.* **101** 980–990. MR2324109 https://doi.org/10.1198/016214506000000672

KOTZ, S., KOZUBOWSKI, T. J. and PODGÓRSKI, K. (2001). *The Laplace Distribution and Generalizations*: *A Revisit with Applications to Communications*, *Economics*, *Engineering*, *and Finance*. Birkhäuser, Inc., Boston, MA. MR1935481 https://doi.org/10.1007/978-1-4612-0173-1

KOZUMI, H. and KOBAYASHI, G. (2011). Gibbs sampling methods for Bayesian quantile regression. *J. Stat. Comput. Simul.* **81** 1565–1578. MR2851270 https://doi.org/10.1080/00949655.2010.496117

LEE, C. C. (2021). Weather whiplash: Trends in rapid temperature changes in a warming climate. *Int. J. Climatol.* **42** 4214–4222. https://doi.org/10.1002/joc.7458

LI, G., LI, Y. and TSAI, C.-L. (2015). Quantile correlations and quantile autoregressive modeling. *J. Amer. Statist. Assoc.* **110** 246–261. MR3338500 https://doi.org/10.1080/01621459.2014.892007

LUM, K. and GELFAND, A. E. (2012). Spatial quantile multiple regression using the asymmetric Laplace process. *Bayesian Anal.* **7** 235–258. MR2934947 https://doi.org/10.1214/12-BA708

MCKINNON, K. A. and POPPICK, A. (2020). Estimating changes in the observed relationship between humidity and temperature using noncrossing quantile smoothing splines. *J. Agric. Biol. Environ. Stat.* **25** 292–314. MR4132962 https://doi.org/10.1007/s13253-020-00393-4

NAVARRO-SERRANO, F., LÓPEZ-MORENO, J. I., AZORIN-MOLINA, C., ALONSO-GONZÁLEZ, E., TOMÁS-BURGUERA, M., SANMIGUEL-VALLELADO, A., REVUELTO, J. and VICENTE-SERRANO, S. M. (2018). Estimation of near-surface air temperature lapse rates over continental Spain and its mountain areas. *Int. J. Climatol.* **38** 3233–3249. https://doi.org/10.1002/joc.5497

NEELON, B., LI, F., BURGETTE, L. F. and BENJAMIN NEELON, S. E. (2015). A spatiotemporal quantile regression model for emergency department expenditures. *Stat. Med.* **34** 2559–2575. MR3368401 https://doi.org/10.1002/sim.6480

PEÑA-ANGULO, D., GONZALEZ-HIDALGO, J. C., SANDONÍS, L., BEGUERÍA, S., TOMAS-BURGUERA, M., LÓPEZ-BUSTINS, J. A., LEMUS-CANOVAS, M. and MARTIN-VIDE, J. (2021). Seasonal temperature trends on the Spanish mainland: A secular study (1916–2015). *Int. J. Climatol.* **41** 3071–3084. https://doi.org/10.1002/joc.7006

PETERS, G. W. (2018). General quantile time series regressions for applications in population demographics. *Risks* **6** 97. https://doi.org/10.3390/risks6030097

REICH, B. J. (2012). Spatiotemporal quantile regression for detecting distributional changes in environmental processes. *J. R. Stat. Soc. Ser. C. Appl. Stat.* **61** 535–553. MR2960737 https://doi.org/10.1111/j.1467-9876.2011.01025.x

REICH, B. J., FUENTES, M. and DUNSON, D. B. (2011). Bayesian spatial quantile regression. *J. Amer. Statist. Assoc.* **106** 6–20. MR2816698 https://doi.org/10.1198/jasa.2010.ap09237

SRIRAM, K., RAMAMOORTHI, R. V. and GHOSH, P. (2013). Posterior consistency of Bayesian quantile regression based on the misspecified asymmetric Laplace density. *Bayesian Anal.* **8** 479–504. MR3066950 https://doi.org/10.1214/13-BA817

TAN, X., GAN, T. Y. and CHEN SHU LIU, B. (2019). Modeling distributional changes in winter precipitation of Canada using Bayesian spatiotemporal quantile regression subjected to different teleconnections. *Clim. Dyn.* **52** 2105–2124. https://doi.org/10.1007/s00382-018-4241-0

TOKDAR, S. T. and KADANE, J. B. (2012). Simultaneous linear quantile regression: A semiparametric Bayesian approach. *Bayesian Anal.* **7** 51–72. MR2896712 https://doi.org/10.1214/12-BA702

YANG, Y. and HE, X. (2015). Quantile regression for spatially correlated data: An empirical likelihood approach. *Statist. Sinica* **25** 261–274. MR3328814

YANG, C., LI, L. and XU, J. (2018). Changing temperature extremes based on CMIP5 output via semi-parametric quantile regression approach. *Int. J. Climatol.* **38** 3736–3748. https://doi.org/10.1002/joc.5524

YANG, Y. and TOKDAR, S. T. (2017). Joint estimation of quantile planes over arbitrary predictor spaces. *J. Amer. Statist. Assoc.* **112** 1107–1120. MR3735363 https://doi.org/10.1080/01621459.2016.1192545

YANG, Y., WANG, H. J. and HE, X. (2016). Posterior inference in Bayesian quantile regression with asymmetric Laplace likelihood. *Int. Stat. Rev.* **84** 327–344. MR3580414 https://doi.org/10.1111/insr.12114

YU, K. and MOYEED, R. A. (2001). Bayesian quantile regression. *Statist. Probab. Lett.* **54** 437–447. MR1861390 https://doi.org/10.1016/S0167-7152(01)00124-9

ZHANG, H. (2004). Inconsistent estimation and asymptotically equal interpolations in model-based geostatistics. *J. Amer. Statist. Assoc.* **99** 250–261. MR2054303 https://doi.org/10.1198/016214504000000241